SUPPORTING LAND-USE MAPPING BY USING MULTITEMPORAL THERMAL INFRARED IMAGERY IN CONJUNCTION WITH A SIMPLE DIURNAL TEMPERATURE MODEL *

Ramon Franck, Boris Prinz, Hartwig Spitzer
II. Institut für Experimentalphysik, CENSIS
Universität Hamburg
Mail address: KOGS, Vogt-Kölln-Str. 30, 22527 Hamburg, Germany
Email: franck@kogs.informatik.uni-hamburg.de
WWW: http://kogs-www.informatik.uni-hamburg.de/projects/Censis.html

ABSTRACT

We propose an algorithm for deriving surface specific information from a multitemporal thermal data set with a simple model of the diurnal temperature curve. Based on an analytic solution of the heat conduction equation (Price 1977) this algorithm allows the determination of the thermal inertia and of the linearization coefficients of the outgoing heatfluxes for each pixel of a multitemporal thermal image by fitting the model to the respective temperature values. At least three temperature measurements at different times of one day are needed for that process. For computational convenience we introduce a function representing the ratio of two temperature differences. The determined model parameters are analyzed regarding their usefulness for land-use mapping. The algorithm was tested on a multitemporal multispectral image data set recorded by a DAEDALUS AADS 1268 line scanner. The test site was an agricultural area near the city of Nuremberg, Germany. The data was recorded at 4:30 a.m., 8:30 a.m. and 11:30 a.m. (MET). In order to value the information on surface properties derived by applying this method we related the resulting parameters to NDVI and apparent thermal inertia values. The results show their usefulness for supporting land-use mapping.

1 INTRODUCTION

Remotely sensed thermal data has been used widely to determine surface properties, particularly thermal inertia and surface humidity. Experimental restrictions forced the researchers in the majority of cases to rely on one-time measurements (e.g. (Seguin & Itier 1983)) or day-night-difference temperature images (e.g. (Watson 1982)). Through the launch of hyperspectral satellites in the near future multitemporal thermal data measured at more times of a day can be provided offering new possibilities for thermal image interpretation.

During the Heat Capacity Mapping Mission a model for the diurnal temperature curve was developped which is based on an analytical solution of the heat conduction equation (Price 1977). With that model tedious calculations with numerical models can be avoided. If only two temperature measurements are available (which is the common case for HCMM imagery based investigations) approximations have to be used and the results are of limited validity (Price 1985). Provided with a third temperature measurement the exact model can be used for calculating surface properties yielding additional and more precise information on surface properties.

In this paper we propose an algorithm to fit this analytical model of the diurnal temperature curve to a multitemporal thermal imagery data set recorded at least at three different times of a day. The determined parameters are the

* Presented at the Fourth International Airborne Remote Sensing Conference and Exhibition / 21st Canadian Symposium on Remote Sensing, Ottawa, Ontario, Canada, 21–24 June 1999.

thermal inertia and the linearization coefficients of the outgoing heatfluxes. The latter enable the determination of the mean surface temperature of the observation day and the sum of the latent heatflux and the sensible heatflux at each time of the observation day. The algorithm was tested with multitemporal multispectral image data recorded by the airborne line scanner DAEDALUS AADS 1268. At flight altitudes of 300 m and 900 m the geometric ground resolutions were about one and three meters, respectively.

Calculation of the errors showed the need to average the resulting parameter images over regions of interest. This is not a serious restriction as we are interested in surface properties of agricultural areas and not single pixels. Because of the model's simplicity the determined parameters representing surface properties should only be regarded as *effective* ones and comparisons between modeled values should only be made within one data set. Taking into account these restrictions comparison with NDVI- and apparent thermal inertia (ATI) values showed additional information for land-use mapping. A quantitative analysis is in progress.

2 THERMAL MODEL

Assuming the one-dimensional periodic heating of a uniform half-space of constant thermal properties, the temperature obeys the diffusion equation. The boundary condition can be expressed as (Xue & Cracknell 1995):

$$-K \left.\frac{\partial T(x,t)}{\partial x}\right|_{x=0} = (1-alb)S_0 V \cos Z - R_{\mathrm{surf}} + R_{\mathrm{sky}} - H - LE, \tag{1}$$

where K is the thermal conductivity, $T(x,t)$ the temperature of the half-space in depth x, alb is the surface albedo, $S_0 = 1375\ \mathrm{W/m^2}$ the solar constant, V the atmospheric transmittance, $cosZ = \sin\delta\sin\alpha + \cos\delta\cos\alpha$, δ the solar declination, α the latitude of observation, R_{surf} the emitted longwave radiation, R_{sky} the atmospheric counter radiation, H the sensible heat flux and LE the latent heat flux. An analytic solution of the diffusion equation subject to boundary condition (1) is obtained by Fourier analysis (Carslaw & Jaeger 1959). Therefore the boundary condition has to be linearized:

$$-K \left.\frac{\partial T(x,t)}{\partial x}\right|_{x=0} = (1-alb)S_0 V \cos Z - [A_{\mathrm{c}} + B_{\mathrm{c}} T(0,t)]. \tag{2}$$

A_{c} and B_{c} are the linearization coefficients. After some straightforward calculations the following solution for the surface temperature is obtained (the expression given in (Xue & Cracknell 1995) lacks the coefficient C_0):

$$T(t) = \frac{(1-alb)S_0 V C_0 - A_{\mathrm{c}}}{B_{\mathrm{c}}} + (1-alb)S_0 V \sum_{n=1}^{\infty} C_n \frac{\cos(n\omega t - \delta_n)}{\sqrt{\omega n P^2 + \sqrt{2n\omega}\, B_{\mathrm{c}} P + B_{\mathrm{c}}^2}}. \tag{3}$$

with P thermal inertia and

$$\begin{aligned}
\omega &= 2\pi/(24\ \mathrm{h}), \quad \delta_{\mathrm{n}} = \arctan\left(\frac{\mathrm{P}\sqrt{\mathrm{n}\omega}}{\sqrt{2}\mathrm{B_c} + \mathrm{P}\sqrt{\mathrm{n}\omega}}\right), \\
C_0 &= \frac{1}{\pi}\cos\delta\cos\alpha\sin\left(\frac{\pi}{2} + \sin^{-1}(\tan\delta\tan\alpha)\right) + \frac{1}{\pi}\sin\delta\sin\alpha\left(\frac{\pi}{2} + \sin^{-1}(\tan\delta\tan\alpha)\right) \\
C_1 &= \frac{2}{\pi}\sin\delta\sin\alpha + \frac{1}{2\pi}\cos\delta\cos\alpha[\sin(2\psi) + 2\psi], \quad \psi = \arccos(\tan\delta\tan\alpha) \\
C_n &= \frac{2\sin\delta\sin\alpha}{n\pi}\sin(n\psi) + \frac{2\cos\delta\cos\alpha}{\pi(n^2-1)}[n\sin(n\psi)\cos\psi - \cos(n\psi)\sin\psi], \quad n = 2, 3, \ldots
\end{aligned}$$

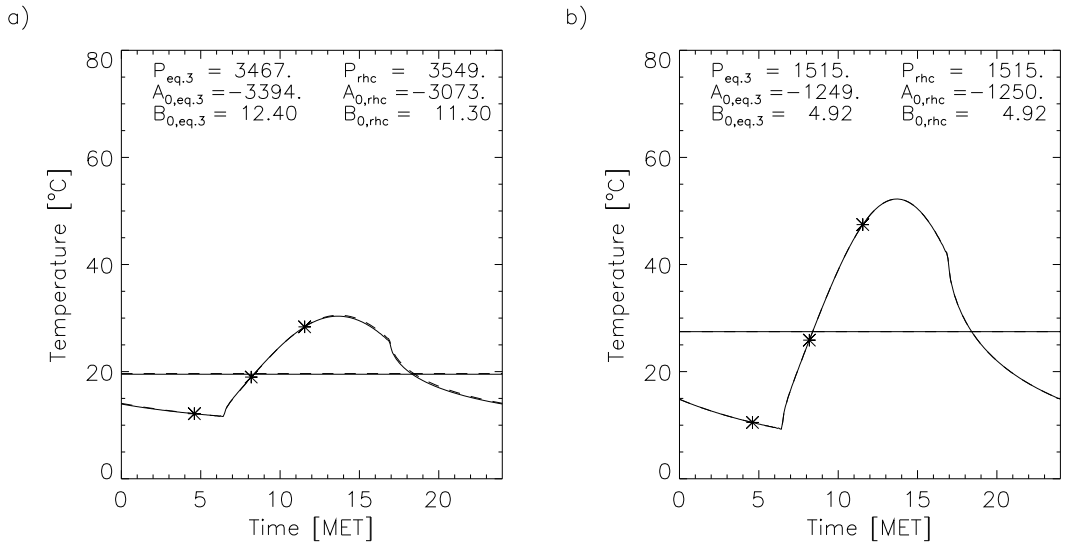

Figure 1: Hypothetical temperature data (asterisks) and modeled temperature curves directly using (3) (solid line) and based on the rhi-function (dashed line, see (5)). The lines at constant temperature levels represent the daily mean temperatures $\overline{T} = (A_c - C_0)/B_c$ [°C]. The units of the parameters are: $[P] = [Jm^{-2}s^{-1/2}K^{-1}]$, $[A_c] = [Wm^{-2}]$ and $[B_c] = [Wm^{-2}K^{-1}]$. The apparent differences between $A_{0,\mathrm{eq.3}}$ and $A_{0,\mathrm{rhi}}$ resp. $B_{0,\mathrm{eq.3}}$ and $B_{0,\mathrm{rhi}}$ in a) do not yield different temperature curves since $A_c + B_c T(t)$ in the respective temperature range and $\overline{T}$ are similar in both cases.

3 CALCULATION OF SURFACE PROPERTIES

Having an appropriate number of temperature measurements at different times of one day one can use the model described in Section 2 to calculate surface properties. This is called an *inverse modeling process*. The parameters in (3) which cannot be determined or at least estimated directly from remote sensing measurements are the linearization coefficients A_c and B_c and the thermal inertia P. Having at least three temperature values per surface resolution cell a non-linear least square fit routine (Brandt 1992) can be used for their determination. The values which have to be provided are that of the surface albedo (which can be determined using the reflective channels of a remote sensing system) and the atmospheric transmittance (usually determined by a radiative transfer computer code like MODTRAN complemented by on-site measurements). This fitting process yields in general a very good agreement between modeled and measured temperature values (Fig. 1).

The prescribed calculation is time-consuming (about 1 min with three measured temperature values on a SparcUltraI with 147 MHz and 160 MB RAM) and therefore cannot be performed for each pixel of a remotely sensed image. The number of fits can be reduced by using the following function which we called the *relative heating index* (rhi):

$$\mathrm{rhi} \equiv \frac{T(t_2) - T(t_1)}{T(t_{\mathrm{ref},2}) - T(t_{\mathrm{ref},1})} \tag{4}$$

From (3) we get:

$$\mathrm{rhi} = \mathrm{rhi}\left(t_1, t_2, t_{\mathrm{ref},1}, t_{\mathrm{ref},2}, \frac{B_c}{P}\right) = \frac{\sum_{n=1}^{\infty} C_n \frac{\cos(n\omega t_2 - \delta_n) - \cos(n\omega t_1 - \delta_n)}{\sqrt{n + \sqrt{2n}/\omega \frac{B_c}{P} + \frac{1}{\omega}\frac{B_c^2}{P^2}}}}{\sum_{n=1}^{\infty} C_n \frac{\cos(n\omega t_{\mathrm{ref},2} - \delta_n) - \cos(n\omega t_{\mathrm{ref},1} - \delta_n)}{\sqrt{n + \sqrt{2n}/\omega \frac{B_c}{P} + \frac{1}{\omega}\frac{B_c^2}{P^2}}}} \tag{5}$$

This function representing the ratio of two temperature differences depends only on one variable, namely the ratio B_c/P. The time parameters $t_1, t_2, t_{ref,1}$ and $t_{ref,2}$ are determined by experimental conditions (the subscript *ref* indicates that standardized measurements like the commonly measured day-night temperature differences can be used as denominator in (4) and an additional temperature measurement in the morning can yield the third value needed for calculation of the numerator). That means that instead of directly fitting the three-parameter function (3) to temperature values the measured temperature data is now transformed into rhi-values for each resolution cell with (4) and then the one-parameter function (5) is used for the fitting process. For computational convenience the upper and lower boundary of the rhi-function (B_c/P=0 resp. $B_c/P \to \infty$) should first be calculated numerically and an interval of allowed rhi-values be defined. Temperature values of pixels having rhi-values outisde this interval cannot be modeled with (3) and would yield irregular results in the following calculation steps. Therefore these pixels have to be excluded from further calculations. The interval of allowed rhi-values should be divided into an appropriate number of sub-intervals (depending on accuracy requirements and available hardware) and a look-up table should be created using the respective averaged rhi-values of each sub-interval for the fitting process. Having determined the B_c/P-values the calculation of A_c, B_c and P is straightforward using (3). Tests have shown a very good agreement between the fitting based directly on (3) and (5) (see Fig. 1).

To draw surface specific information from the determined linearization coefficients A_c and B_c these parameters are used to calculate $\overline{T} = (A_c - C_0)/B_c$ and $HLE(t) \equiv (H + LE)(t) = A_c + B_c T(t) - R^{lin}_{surf} + R_{sky}$ for each image pixel with $\overline{T}$ mean surface temperature of observation day, HLE sum of sensible heatflux and latent heatflux, $R^{lin}_{surf}(T(t)) = -3\sigma\epsilon\overline{T}^4 + 4\sigma\epsilon\overline{T}^3 T(t)$ (linearized Stefan-Boltzmann-Law), R_{sky} atmospheric-counter radiation, ϵ surface emissivity, $T(t)$ calculated with (3) and t the point in time of interest. R_{sky} can be estimated using heuristic formulas or determined by radiative transfer computer codes like MODTRAN, eventually supplemented by ground measurements and radiosonde data.

3.1 DISCUSSION

As the notion of thermal inertia is not well defined for vegetated surfaces and the assumption of a uniform half-space is not tenable in that case all determined values will be regarded as *effective* ones. A problem inherent to the analytical Fourier approach is the averaging of all model parameters for a whole period, i.e. one day. Even if atmospheric conditions are stable, parameters like air temperature and air humidity change during the integration time. Therefore results should only be compared within one data set recorded within 24 hours. For comparing results from data sets recorded at different days a normalization should be applied. Further discussions regarding the usefulness of the Fourier modeling approach can be found in (Watson 1978) or (Price 1985).

Apart from computational convenience the introduction of the rhi-function yields two considerable advantages. First, this function is (within the model assumptions) independent of atmospheric transmissivity and of albedo. So it can be regarded as a surface property with a high degree of normalization which is important for several applications like classification and change detection. Second, pixels having temperature values that cannot be modeled with (3) can easily be excluded by their irregular rhi-values. Reasons for these irregularities are the simplicity of the model and misregistration of the thermal images. A simple improvement of the resulting images can be achieved by using spatial features, i.e. taking into account neighbouring pixels to assign parameters to excluded pixels.

3.2 COMMENT ON THE ERROR

A decisive point in using an algorithm yielding parameters for describing object properties is the calculation of errors. As a first step the error of the underlying data set, i.e. the measured temperature values, has to be determined. The determination of the total error of the calculated parameters described in Section 3 is then straightforward: The error of the fitting-process can be determined by the linearization of the used function, i.e. the rhi-function in our case (Brandt 1992). All other errors can be determined by applying the Gaussian error propagation law.

The errors of P, A_c and B_c are very sensitive to the errors of the measured temperatures. This is due to the

sensitivity of (3) resp. (5) to the B_c/P-values in the range of appropriate B_c/P-values (see Fig. 2). Using the temperature data shown in Figure 1, an assumed absolute error of $1.0°C$ for each temperature measurement yields relative errors of P, A_c and B_c of a) 29%,197%, 183% and b) 12%, 91%, 78% (neglecting errors of other parameters). As these errors are not tolerable for conclusive results and the requirement of more precise temperature measurements cannot be fulfilled by actual sensor platforms, the resulting images must not be interpreted pixel by pixel but the values have to be averaged over regions of interest. Averaging over n pixels yields a reduction of the error by $1/\sqrt{n}$ (according to the Gaussian error propagation law). For a discussion of the errors resulting from inaccurate model assumptions see 3.1.

4 APPLICATION TO AN AGRICULTURAL AREA

4.1 DATA SET

The imagery was recorded during an experiment that took place at the 26 August, 1997, near the city of Nuremberg, Germany. A DAEDALUS AADS 1268 line scanner on board a Dornier Do 228 aircraft was used yielding a multispectral data set consisting of ten reflective bands and one band in the thermal infrared ($8.5 - 13.\mu m$). At flight altitudes of 300 m and 900 m the geometric ground resolution was about one and three meters, respectively. Image flights took place at 4:30, 8:30, 11:30 and 12:30 (MET), in order to measure a characteristic part of the diurnal temperature curve. As the weather conditions changed between the last two measurements, i.e. clouds turned up, the 12:30-dataset is omitted in the following investigations. Atmospheric corrections were performed by using the SENSAT/MODTRAN computer code (Richter 1992) relying on standard atmospheric parameters supplemented by ground measurements of meteorological data and radiosonde data recorded in Amberg (located 60 km in the east of Nuremberg) (Prinz 1998). The emissivity of the surface was assumed to be 0.97 for the whole test site. From the data set a small scene showing an agricultural area was extracted for every overflight (Fig. 3). The early morning image was taken as reference on which the images were registered using Akima local quintic polynomial interpolation (Wiemker 1996).

4.2 RESULTS AND DISCUSSION

The method described in Section 3 was applied to the data set described above. The time parameters in (5) are determined by the experimental conditions: $t_1 = t_{1,\mathrm{ref}} = 4:36$, $t_2 = 8:11$, $t_{2,\mathrm{ref}} = 11:33$ (MET). The transmissivity $V = 0.75$ was calculated by MODTRAN2. From numerical calculations (B_c/P=0 resp. $B_c/P \to \infty$) we get $\mathrm{rhi} \in [0.345, 0.649]$. As the rhi-function is continuous and monotonically increasing with growing B_c/P-values (see Fig. 2), no local extrema can mislead the fitting routine and the result represents the best overall solution. For the calculation of the errors we used a total error of the measured temperatures of $2.0°C$ (Prinz 1998). Errors of other parameters were neglected.

$HLE(t)$ is calculated for $t = 12:00$ MET, for we have radiosonde data at this time (see Section 4.1) enabling a precise determination of R_{sky} (see Section 3). Figure 4 shows the resulting images. Note that regions that seem to be coherent in the albedo image can in general be found as coherent regions in the resulting images (not taking into account excluded pixels). From the resulting thermal inertia image we defined some regions of interest (see Fig. 4, for comparison these regions are also drawn in the albedo image in Figure 3) and calculated the mean values of the modeled parameters (Table 1). The errors of the $\overline{T}$- and HLE-values are very large and must be reduced by averaging over larger areas. Disregarding the errors a comparison to ground measurements (e.g. (Parlow 1998)) yields an overall agreement regarding their magnitude.

To relate the values of P, $\overline{T}$ and HLE to more commonly used concepts we calculated the correlation coefficients with the NDVI- and apparent thermal inertia (*ATI*) values for each image pixel (see Table 2). As multiplicative constants do not affect the correletaion coefficient, we used the following definition: $ATI = (1 - alb)/(T(11:33) - T(04:36))$. The correlation coefficients of about 0.6 between ATI and $HLE(12:00)$ show an overall agreement between these concepts but indicate the achievement of additional information using the latter ones. Absolute correlation coefficients smaller than 0.4 indicate clearly distinct information sources.

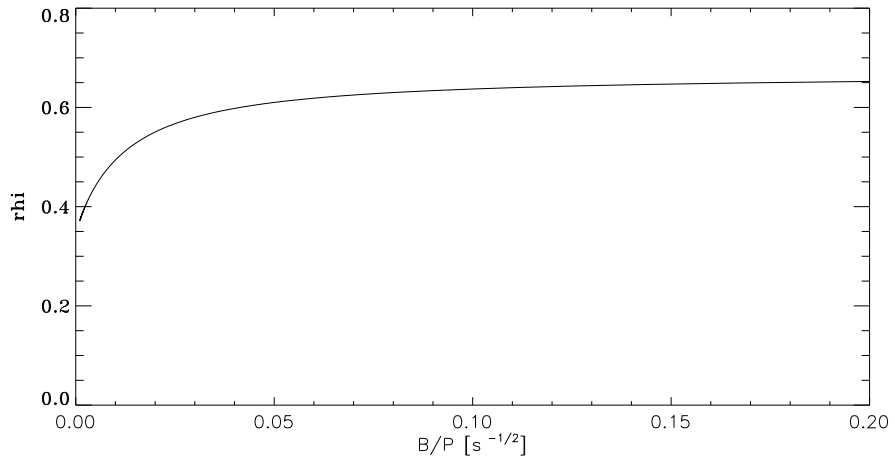

Figure 2: rhi-values as a function of B_c/P. The time parameters are $t_1 = t_{1,\mathrm{ref}} = 4:36, t_2 = 8:11, t_{2,\mathrm{ref}} = 11:33$ (MET).

Table 1: Determined thermal inertia, $\overline{T}$- and HLE-values for some regions of interest (see Fig. 4).

	P $[\mathrm{J/(m^2 s^{1/2})K}]$	A_c $[\mathrm{W/m^2}]$	B_c $[\mathrm{W/m^2/K}]$	$\overline{T}$ [°C]	$HLE(12:00)$ $[\mathrm{W/m^2}]$
Area 1	$2746. \pm 73.$	$-6279. \pm 403.$	22.2 ± 2.4	$21. \pm 49.$	$327. \pm 1161.$
Area 2	$1258. \pm 4.$	$-1768. \pm 35.$	6.6 ± 0.2	$29. \pm 11.$	$126. \pm 102.$
Area 3	$1019. \pm 37.$	$-6219. \pm 417.$	22.1 ± 2.5	$18. \pm 34.$	$386. \pm 1208.$
Area 4	$1887. \pm 19.$	$-3187. \pm 115.$	11.5 ± 0.7	$23. \pm 20.$	$221. \pm 336.$
Area 5	$1340. \pm 24.$	$-4861. \pm 223.$	17.4 ± 1.3	$19. \pm 22.$	$353. \pm 648.$
Area 6	$1819. \pm 109.$	$-7806. \pm 853.$	27.5 ± 5.1	$19. \pm 57.$	$381. \pm 2459.$

Table 2: Correlation coefficients for the whole test scene.

	P	$\overline{T}$	$HLE(12:00)$
NDVI	0.18	-0.68	0.52
ATI	0.58	-0.67	0.58

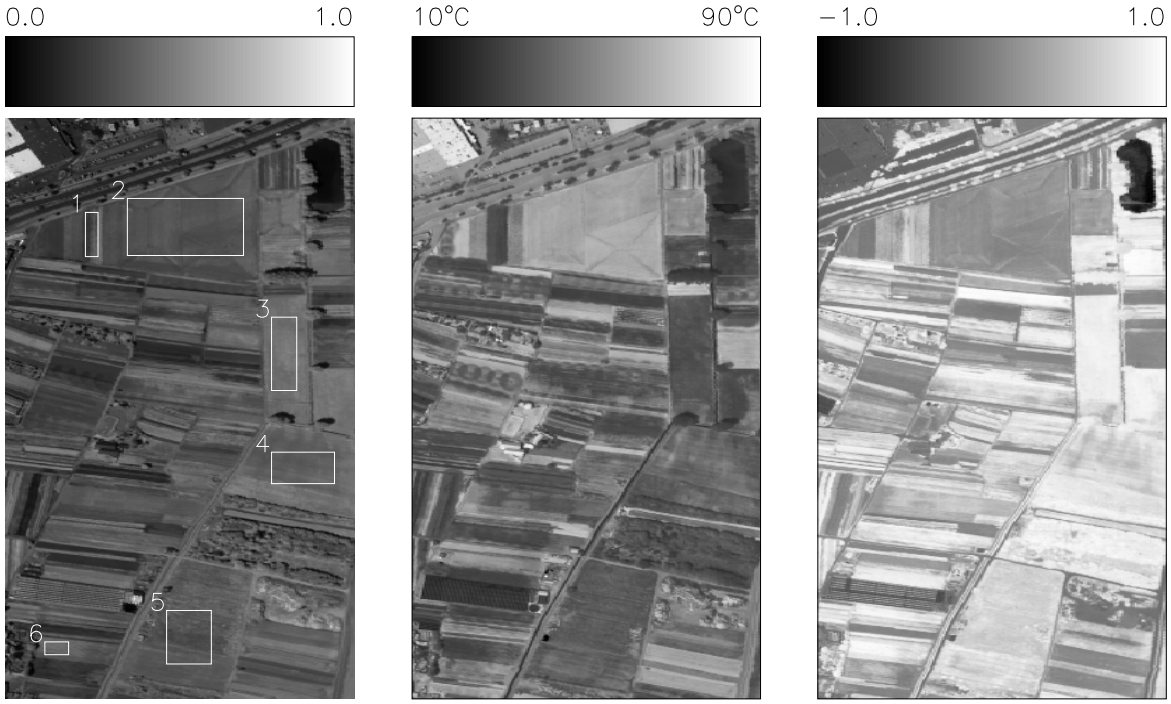

Figure 3: Albedo-, temperature (11:33)- and NDVI- image of the test scene.

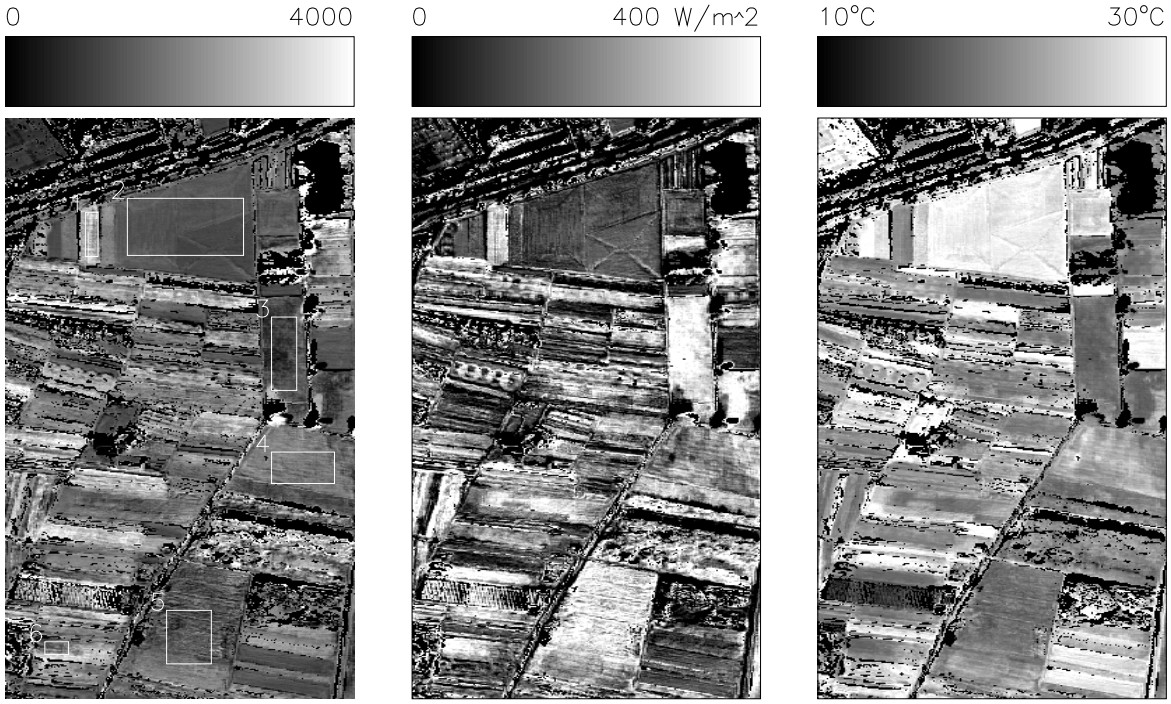

Figure 4: Thermal inertia- (unit: $[\mathrm{J}/(\mathrm{m}^2\mathrm{s}^{1/2})\mathrm{K}]$), $HLE(12:00)$- and $\overline{T}$-images; excluded pixels are colored black.

5 CONCLUSIONS

In this paper we developed a method to fit a simple analytical model of the diurnal surface temperature curve to a multitemporal thermal data set consisting at least of temperature measurements at three different times of one day. This procedure yields three parameters for each image pixel describing thermal properties of the underlying surface, i.e. the thermal inertia and the two linearization coefficients of the outgoing surface fluxes. For interpretation purposes, the latter ones can be used to calculate the daily mean temperature and the sum of the sensible heatflux and the latent heatflux. Because of the model's simplicity and the algorithm's sensitivity towards errors of the measured temperature data these parameters should only be used for investigations within one data set and of large areas. Tests with a multitemporal multispectral data set recorded by a DAEDALUS AADS 1268 line scanner over an agricultural area showed that additional information is achieved in comparison to NDVI and ATI values.

ACKNOWLEDGEMENT

This work was supported by the Volkswagen-Stiftung. The image flights were conducted in collaboration with the German Aerospace Center (DLR Weßling, München), particularly with the help of Volker Amann and Manfred Schröder. We thank Rudolf Richter (DLR) for discussions and support concerning atmospheric corrections.

REFERENCES

Brandt, S. (1992). *Datenanalyse*. BI-Wissenschaftsverlag, Mannheim, Leipzig, Wien, Zürich, 1992.

Carslaw, H. S. and J. C. Jaeger (1959). *Conduction of Heat in Solids*. New York: Oxford University Press, 1959.

Parlow, E. (1998). Net Radiation in Urban Areas. In Gudmandsen, P., editor, *Future Trends in Remote Sensing*, pages 221–226. Balkema-Publishers Rotterdam, 1998.

Price, J. C. (1977). Thermal Inertia Mapping: A New View of the Earth. *Journal of Geophysical Research* **82** (18), 2582–2590, 1977.

Price, J. C. (1985). On the Analysis of Thermal Infrared Imagery: The Limited Utility of Apparent Thermal Inertia. *Remote Sensing of Environment* **18**, 59–73, 1985.

Prinz, B. (1998). Thermalkartierung städtischer Gebiete anhand von Multispektralbildern , Diplomarbeit, Universität Hamburg, II. Institut für Experimentalphysik, CENSIS-Report 31-98., 1998.

Richter, R. (1992). *Radiometrische Auslegung von Sensoren und quantitative Auswertung von Fernerkundungsdaten im optischen Spektralbereich*. PhD thesis, German Aerospace Research Establishment (DLR), Oberpfaffenhofen, 1992.

Seguin, B. and B. Itier (1983). Using Midday Surface Temperature to estimate Daily Evaporation from Satellite Thermal IR Data. *International Journal of Remote Sensing* **4** (2), 371–383, 1983.

Watson, K. (1978). Thermal Phenomena and Energy Exchange in the Environment. In *Mathematical and Physical Principles of Remote Sensing*, pages 109–174. CNES. Strasbourg, 1978.

Watson, K. (1982). Regional Thermal-Inertia Mapping from an Experimental Satellite. *Geophysics* **47** (12), 1681–1687, 1982.

Wiemker, R. (1996). Registration of Airborne Scanner Imagery Using Akima Local Quintic Polynomial Interpolation. In *Proceedings of the Second International Airborne Remote Sensing Conference and Exhibition, San Francisco*, Ann Arbor, 1996, volume III, pages 210–219. Environmental Research Institut of Michigan.

Xue, Y. and A. P. Cracknell (1995). Advanced Thermal Inertia Modelling. *International Journal of Remote Sensing* **16** (3), 431–446, 1995.